 DT# 48106 QA:NA 7/5/06 CB

Mechanical degradation of emplacement drifts at Yucca Mountain—A modeling case study. Part I: Nonlithophysal rock

M. Lin[a,1], D. Kicker[a,2,*], B. Damjanac[b], M. Board[b], M. Karakouzian[c]

[a]*Bechtel SAIC Company, 1180 Town Center Dr, Las Vegas, NV 89144, USA*
[b]*Itasca Consulting Group Inc., 111 Third Avenue South, Suite 450, Minneapolis, MN 55401, USA*
[c]*University of Nevada, Department of Civil and Environmental Engineering, 4505 Maryland Parkway, Box 454015, Las Vegas, NV 89154, USA*

Abstract

This paper outlines rock mechanics investigations associated with mechanical degradation of planned emplacement drifts at Yucca Mountain, which is the designated site for the proposed U.S. high-level nuclear waste repository. The factors leading to drift degradation include stresses from the overburden, stresses induced by the heat released from the emplaced waste, stresses due to seismically related ground motions, and time-dependent strength degradation. The welded tuff emplacement horizon consists of two groups of rock with distinct engineering properties: nonlithophysal units and lithophysal units, based on the relative proportion of lithophysal cavities. The term 'lithophysal' refers to hollow, bubble like cavities in volcanic rock that are surrounded by a porous rim formed by fine-grained alkali feldspar, quartz, and other minerals. Lithophysae are typically a few centimeters to a few decimeters in diameter. Part I of the paper concentrates on the generally hard, strong, and fractured nonlithophysal rock. The degradation behavior of the tunnels in the nonlithophysal rock is controlled by the occurrence of keyblocks. A statistically equivalent fracture model was generated based on extensive underground fracture mapping data from the Exploratory Studies Facility at Yucca Mountain. Three-dimensional distinct block analyses, generated with the fracture patterns randomly selected from the fracture model, were developed with the consideration of in situ, thermal, and seismic loads. In this study, field data, laboratory data, and numerical analyses are well integrated to provide a solution for the unique problem of modeling drift degradation.

Keywords: Drift degradation; Rockfall; Discontinuum numerical modeling; Yucca Mountain; Nuclear waste

---

[1] Present address: Shell Exploration & Production Company, Unconventional Resources, Two Shell Plaza, 777 Walker Street, Houston, TX 77002, USA

[2] Present address: SM Stoller Corporation, 1180 Town Center Dr, Las Vegas, NV 89144, USA

* Corresponding author. Tel.: +1 702 295 4938; fax: +1 702 295 3123.
E-mail address: dwayne_kicker@ymp.gov (D. Kicker).

1. Introduction

Yucca Mountain is located on federal land on and adjacent to the Nevada Test Site in Nye County, Nevada. It has undergone comprehensive site characterization activities for gathering site information beginning in the early 1980's. In 2002, the site was designated as the U.S. repository for high-level nuclear waste.

Degradation of underground openings as a function of time is a natural and expected occurrence for any subsurface excavation. Over time, changes occur to both the stress condition and the strength of the rock mass due to several interacting factors. Once the factors contributing to degradation are characterized, the effects of drift degradation can typically be mitigated through appropriate design and maintenance of the ground support system. However, for the emplacement drifts of the geologic repository at Yucca Mountain, it is necessary to characterize drift degradation over a 10,000-year period or more, which is well beyond the functional period of the ground support system. This paper provides a summary of the study of the stability of repository excavations in nonlithophysal[3] tuff and potential mechanical degradation under the action of in situ, thermal, and seismic stresses during the first 10,000 years of repository performance. A study of the stability of repository excavations in lithophysal[3] tuff is provided in Part II [1].

2. Site geology and geotechnical characteristics of the host rock

The proposed repository will be located in tuff that was deposited by a series of volcanic eruptions approximately 12.8 million years ago. The lithostratigraphy and geologic evolution of the Yucca Mountain site is described in *Yucca Mountain Site Description* [2]. The water table at Yucca Mountain is approximately 500 m to 800 m below the surface at the repository location. The deep water table and thick unsaturated zone result from the low infiltration rate of surface water due to low annual rainfall and high rates of evaporation and transpiration.

Site-specific characteristics of the rock units of the Topopah Spring Tuff that constitute the host rock at the repository horizon are found in the geologic mapping of those units in both the main drift and ramps of the

[3] The term 'lithophysal' refers to hollow, bubble like cavities in volcanic rock that are surrounded by a porous rim formed by fine-grained alkali feldspar, quartz, and other minerals. Lithophysae are typically a few centimeters to a few decimeters in diameter.

Exploratory Study Facility (ESF) and the Enhanced Characterization of the Repository Block (ECRB) Cross-Drift (Fig. 1). The units that comprise the host rocks of the repository horizon are zones of the crystal-poor member of the Topopah Spring Tuff. The host rocks are shown schematically in Fig. 2. In descending order (by depth), the repository horizon consists of the lower part of the upper lithophysal zone (Tptpul), the middle nonlithophysal zone (Tptpmn), the lower lithophysal zone (Tptpll), and the lower nonlithophysal zone (Tptpln). The repository host rock units can be categorized into two general engineering classifications: nonlithophysal units (Tptpmn and Tptpln) and lithophysal units (Tptpul and Tptpll), based on the relative proportion of lithophysal cavities. According to current design, the entire repository is to be located in densely welded and crystallized volcanic tuff with approximately 85% of the repository in lithophysal tuff and 15% in nonlithophysal tuff. The nonlithophysal units are generally hard, strong, fractured rocks with matrix porosities of 10% or less. Fractures that formed during the cooling process are the primary structural features found in these units. In contrast, the lithophysal units have significantly fewer fractures of significant continuous length (i.e., trace length greater than 1 m), but have relatively uniformly distributed porosity in the form of lithophysal cavities. Lithophysal porosity in the Tptpul and Tptpll is generally on the order of less than 10% to about 30% by volume. The groundmass that makes up the rock matrix in the lithophysal units is mineralogically the same as the matrix of the nonlithophysal units, but is heavily fractured with small-scale (lengths of less than 1 m) fractures in the Tptpll; however, it is relatively fracture-free in the Tptpul.

The rock matrix material is a typical fine-grained volcanic rock of silica content with a mean unconfined compressive strength of approximately 180 MPa [3]. The structure of the rock mass defines the properties and overall mechanical response of the rock mass to thermal and mechanical loading. The fracture geometry and properties in the nonlithophysal rocks and the degree of porosity (total and lithophysal) in the lithophysal subunits are the primary geologic structural features that impact rock mass behavior. More detailed description on the effect of lithophysal cavities on the rock mechanical behavior is provided in Part II.

Geotechnical mapping of fractures has been performed in the ESF and the ECRB Cross-Drift [4,5]. Fig. 3 presents a schematic of the Topopah Spring Tuff Formation, illustrating the general occurrence of fracturing and lithophysae in the various subunits of the repository host horizon. The occurrence of fractures and lithophysae are roughly inversely proportional as demonstrated quantitatively in Fig. 3, where the fracture density (fractures with trace length greater than 1 m) determined from detailed line mapping and the

approximate percentage of lithophysal porosity in the ECRB Cross-Drift are shown. The density of fractures with trace length greater than 1 m is significantly larger in the nonlithophysal rock (20 to 35 fractures/10 m), compared to the lithophysal rock (5 fractures/10 m). Conversely, lithophysae are sparse in the nonlithophysal units.

The field fracture database, constructed from mapping in the ESF and ECRB Cross-Drift during tunneling operations, consists of full-periphery maps and detailed line surveys of all fractures with length of one meter or greater. In total, a database of more than 35,000 fracture descriptions is available. In summary, there are four sets of fractures in the Tptpmn with the geometrical and surface characteristics shown in Table 1.

The low-angle vapor-phase partings are relatively continuous structures seen throughout the nonlithophysal rock. These continuous, but anastomosing fractures are subparallel to the dip of the rock unit, and are filled with concentrations of vapor-phase mineralization (primarily tridymite and cristobalite). The surfaces are rough on a small scale and, unlike the subvertical fractures, have cohesion as a result of the mineral filling.

Rotary and direct shear tests were conducted on natural rock fractures from core samples in the repository host units. An average cohesion of 0.9 MPa and peak friction angle of 41° was obtained from the rotary shear tests. The results from the direct shear tests are divided into two groups: one represents the subvertical cooling joints and the other for the vapor-phase parting. The average cohesion and peak friction angle are 0.3 MPa and 34° for the cooling joints and 0.7 MPa and 44° for the vapor-phase parting.

3. General approach

The nature of the fracture geometry governs the estimates of the stability and degradation of the nonlithophysal rock mass, particularly under the action of seismic shaking, as well as estimates of the support performance and level of required ground support. The blocks of nonlithophysal rock are significantly stronger than the in situ and thermally induced stresses, and thus the problem of modeling this material is essentially one of elastic blocks separated by fracture surfaces. Therefore, in modeling the stability of the tunnels and the rockfall that may occur from the applied load, the fracture geometry and surface properties are of primary importance. Three-dimensional discontinuum numerical methods are required for correct representation of the degradation mechanism. The approach to modeling mechanical degradation and rockfall from combined in situ, thermal, and seismic loading in nonlithophysal rock is illustrated in Fig. 4. This approach involves modeling of emplacement drifts excavated within the stochastically defined, representative fractured rock mass volume, followed by application of in situ, thermal, and seismic load. A large number of parameter studies are conducted in which the tunnel location (and fracture geometry), rock fracture surface properties, and loading conditions are varied to derive an appropriate range of performance rèsponse (in terms of rockfall mass, volume, and opening shape) that is indicative of the possible geologic conditions at depth. Sensitivity study of the thermal properties and preclosure heat removal ratio (considering both 90% and 70% heat removal cases) is also included.

The time to failure for intact nonlithophysal rock blocks due to stress corrosion shows significantly less time dependency than for the lithophysal rock based on the laboratory long-term testing data [6]. Therefore, insignificant time-related fracture growth is expected in the intact rock blocks in nonlithophysal units. Contrary to the lithophysal rock, time-dependent strength degradation within the intact block is not considered for the nonlithophysal rock.

Ground support is not considered in the mechanical degradation models in this study. The rock blocks predicted in this study are, therefore, blocks that fail in an unsupported opening. This modeling approach leads to a conservative prediction of unstable blocks for the time frame before the closure of the repository (i.e., more blocks will be predicted to fail in the model that would otherwise be supported and remain stable

with ground support). During the postclosure period, ground support will degrade and eventually fail. Not including ground support in the rockfall models is realistic for the postclosure period.

4. Development of fracture geometries for nonlithophysal rock

The development of a stochastically defined fracture system, representative of the actual rock mass, is accomplished using the FracMan program [7]. The existing fracture mapping database provides the basic input to the FracMan program, which develops sets of planar, circular fracture planes that conform to the statistical variability of the geometric characteristics of the input data. Statistical models are fitted to the various geometric characteristics of each fracture set in the database, followed by generation of representative fracture sets. These representative fractures are then back-checked against the statistical variability and geologic realism of the field data to achieve an acceptable facsimile. Details of this process are described in *Drift Degradation Analysis* [6]. A three-dimensional representative rock mass cube, 100 m on a side, is generated using FracMan and composed of the matrix blocks defined by approximately 90,000 fractures. Each fracture is described by its centroid coordinate, dip, dip direction, and radius. These geometric properties are used as direct inputs to the distinct element code 3DEC [8] for development of a block geometry within which emplacement drifts can be randomly excavated.

The constructed FracMan fracture region is calibrated to the observed data for orientation and its dispersion, size and its distribution, and intensity (as measured by interfracture distance) and its distribution on a set-by-set basis. In addition, any biases due to sampling were effectively removed by using the same sampling style as the observed data collection when comparing the synthetic and the observed data sets. The detailed line survey data in the Tptpmn unit are used to condition FracMan to develop representative fracture trace lengths and spacings. Table 2 displays the mean orientation of the sets, a comparison of median fracture radius converted to diameter and median trace length, and intensity (median spacing) from FracMan and median spacing from the detailed line surveys. A direct comparison between actual full periphery geologic maps from the ESF to synthetic full periphery geologic maps from FracMan is given in Fig. 5. This comparison ensures that the synthetic fracture geometries are not only quantitatively validated, but similar from a geological perspective as well.

5. Distinct block dynamic and thermal-mechanical analyses

A total of 50 emplacement drifts are randomly located and "excavated" within the 100 m cube rock mass generated by FracMan, such that the stochastic nature of the jointed medium and its impact on rockfall is adequately sampled. A random emplacement drift centroid coordinate is chosen within the cube, and a 25 m × 25 m × 25 m volume, oriented at the emplacement drift 72° azimuth, is extracted to contain the model emplacement drift (Fig. 6). The dimension of the model is selected to optimize the time required for analysis and the ability of the model to accurately predict rockfall. Sensitivity of the model dimension to the outcome of rockfall prediction has been evaluated and concluded to be adequate. Within each emplacement drift, a rigid, rectangular block representing the drip shield[4] is affixed to the invert of the tunnel.

Because the fractures within the Tptpmn are nonpersistent in nature (with median trace lengths of approximately 3 m [Table 2], which is smaller than the 5.5-m tunnel diameter), many fractures are of insufficient length to form a regular block. An algorithm was developed for applying the FracMan fracture geometry to the 3DEC model. Previous versions of the 3DEC program were set up to only efficiently handle through-going joint planes. The new algorithm allows incomplete fractures to be cut within a block, or to terminate against other fractures, thus creating realistic fracture patterns within the rock mass. In other words, portions of a fracture plane could be assigned a standard Coulomb slip behavior, whereas others could be bonded to the opposing surface with the strength of the adjacent rock blocks, thereby creating fractures that have rock "bridges" along their surface. In this case, the rock bridge acts as a strong bond along the fracture surface, but can still fail in shear or tension if the stresses so dictate. In this manner, it is possible to represent a discontinuous fracture system, but one in which breakage of solid rock can occur. The resulting blocks within the 3DEC model are fully deformable as they are subdivided into tetrahedral finite difference zones with a linear elastic constitutive model. The 3DEC model uses a fully dynamic solution algorithm to solve the laws of motions for the blocks, subject to contact restraints with surrounding blocks. The gridpoints along

[4] A titanium drip shield is planned to be installed over the waste packages prior to repository closure. The purpose of the drip shield is to divert any moisture that might drip around the waste packages to the drift floor. The drip shields are designed to maintain their function in the event of rockfall.

the fracture surfaces act as contact points across which forces are transmitted, subject to shear and tensile yield conditions.

Other enhancements added to 3DEC for rockfall modeling include: (a) implementation of the "free field" boundary to provide a "quiet" or "non-reflecting" boundary for dynamic analysis with superposition of the P and S wave motions, and (b) partial density scaling for dynamic analysis. These enhancements enable an efficient solution for the dynamic simulation of the seismic wave propagation in three-dimensional media.

5.1. Dynamic analysis with seismic loads

Input properties for the distinct block 3DEC model involve both the fracture and block (intact) properties. Table 3 lists the base case properties used in 3DEC. A linear elastic model is used for the block material, whereas Coulomb slip criterion is used to represent joint mechanical behavior. This approach is used to obtain a conservative (i.e., increased) estimate of the block volume. Breaking and spalling of the rock inside the blocks are expected considering the large amplitude of seismic waves for postclosure ground motions. Although the shallow-dipping vapor-phase parting consists of higher cohesive material, a single set of joint mechanical properties are used for the joint sets for conservatism (i.e., more rockfall will be produced). Coulomb slip criterion is also used for the intact bridges between adjacent fractures, where the intact cohesion and friction is assigned for the bridge strength.

The initial state of stress was included at the model consolidation stage. The vertical component of in situ stress (the major principal stress) is approximated as 7 MPa considering an overburden depth of 300 m. The horizontal components of in situ stress (the minor and intermediate principal stresses) are simplified to be 3.5 MPa based on an average horizontal-to-vertical stress ratio of 0.5. The in situ stress for each emplacement drift will vary depending on the cover depth on top of the drift. The approximated values assigned for the in situ stress are adequate and the results are insensitive judging the magnitude of the induced seismic and thermal stress.

Site-specific ground motions were developed for Yucca Mountain through use of a formal process of expert elicitation resulting in development of a Probabilistic Seismic Hazard Assessment (PSHA)[5]. Site-specific ground motion time histories for four levels of annual probability of exceedance, 1×10^{-4}, 1×10^{-5}, 1×10^{-6}, and 1×10^{-7}, were examined.

A total of 15 sets of ground motion time histories were developed at the repository horizon for each annual postclosure hazard level. The multiple sets ensure a reasonable distribution of spectral shapes and time history duration. For each set of ground motions, two horizontal components (H1 and H2) and one vertical component (V) of acceleration, velocity, and displacement are supplied. The motions include the effects of the free surface reflections, and, thus, the 3DEC model does not need to account for them. Fig. 7 shows the H1 velocity time history for four annual hazard levels. In running the 3DEC simulation, the duration of the seismic time histories was truncated to a duration bracketed the 5% and 95% points in the energy buildup as measured by Arias Intensity (an estimate of energy delivered to the structures), as shown in Fig. 7. The amplitude of the peak ground acceleration, velocity, and displacement, and the seismic-induced far-field stress for one of the ground motion sets from each hazard level are provided in Table 4.

Nonreflecting vertical and upper model boundaries in 3DEC allow the wave to pass through the model, and free-field boundaries on the vertical sidewalls of the model prevent damping and distortion along the vertical sidewalls of the incoming wave. No material damping[6], in addition to that supplied by sliding on fracture surfaces, is supplied to the model. Prior to use of the model for examination of drift degradation, seismic wave propagation of models without tunnels was run to ascertain that the wave passed through the model without significant distortion.

A goal of these analyses is to provide an estimate of seismically induced rockfall that is derived from an adequate sampling of the variability of fracture geometries and ground motion time histories. A simple Latin Hypercube sampling scheme was used for the pairing of ground motion and fracture modeling region [10]. A

---

[5] The ground motion hazard determined in the PSHA expert elicitation is unbounded. Because the ground motion experts characterized aleatory variability in ground motion using unbounded lognormal distributions, as the PSHA calculations are extended to lower and lower annual probabilities of exceedance, the mean ground motions increase without bound, eventually reaching levels that are not credible. An analysis was conducted to determine a bound to peak ground velocity (PGV) at the repository level based on the shear strain increments (relative to the in situ stress state) required to fracture the Tptpll rock [9]. The bound to PGV at the repository level has been shown, based on physical strain limitations of the lithophysal rock mass, to be approximately 4 m/s. The unbound velocity time histories were used in this study for conservatism.

total of 50 sets of paired fracturing realizations (i.e., drift centroid locations) and ground motion data were made for each postclosure annual exceedance frequency. For each of these analyses, a base case of block and fracture material properties were used so that the variability of the rockfall response was then a function of the fracture geometry and ground motion variability only. The base case rock and fracture properties are given in Table 3. The adequacy of 50 analyses for representation of the variability of rockfall (at each exceedance level) was verified by calculation of the cumulative mean and standard deviation of rockfall parameters for successive analyses. The mean and standard deviation of rockfall mass does not change after approximately 30 runs.

The results of the seismic analyses are presented in terms of rockfall impact and drift profile. The former provides inputs for the drip shield and waste package design and the later is for seepage consideration. Fig. 8 shows typical blocks impacting the drip shield in the 3DEC dynamic simulation. The block representing the drip shield is anchored at the invert, and is included in the model to record the information on the locations and relative velocities for rockfall impact. Summary histograms for the rockfall impact information with 1×10^{-6} annual probability of exceedance earthquakes are presented in Fig. 9. Also included in each histogram plot is the cumulative frequency of occurrence. The block mass, impact momentum and impact energy show the trend of negative exponential distribution with most of the data concentrated on the low end of the data range. The impact velocity shows a typical bell shape for the normal distribution. The distribution centers around 3 m/s with a standard deviation of approximately 1.7 m/s. The relatively low impact velocities indicate that block fallout is mainly due to gravitational freefall. Differential acceleration or energy trapping to induce high ejection velocity is not observed.

Rockfall analyses were also completed for ground motions with 1×10^{-4}, 1×10^{-5}, and 1×10^{-7} annual exceedance probabilities. The 1×10^{-4} ground motion includes one ground motion set with 32 simulations. A total of 44 cases was conducted for 1×10^{-7} motions, as convergence of the median rock block size was evident after this number of analyses. Fig. 10 shows a comparison of histograms of block mass for all four ground-motion results. Essentially, the results show that all motions result in the same general distribution of block sizes with mean block masses of less than 0.2 metric tons, and a negative exponential distribution.

---

[6] 0.3% of critical damping was used in a few analyses for numerical stability purposes.

Fig. 11 presents correlation of rockfall volume per 3DEC simulation with peak ground velocity (PGV in H1 direction). At any given level of PGV, the variability in rockfall based on the variability in fracture pattern and ground motion frequency characteristics results in a fairly wide distribution in response. Although no strong relationship is observed between rockfall volume and PGV, a roughly linear relationship exists between the upper bound to rockfall volume and PGV on this semi-log plot. The fracture pattern is the predominant mechanism for variability in rockfall at a given level of PGV.

Table 5 compares rockfall statistics for the different annual probabilities of ground motion exceedance. Due to the variable number of runs, the important comparison statistic is the number of blocks per kilometer, which shows an increase from 535 blocks for 1×10^{-4} ground motion to 3,079 blocks for 1×10^{-7} ground motion.

The three-dimensional depiction of an emplacement drift after seismic shaking provides a physical perspective for the impact of seismically induced rockfall on the drift profile. Fig. 12 shows the rockfall profile for the case showing the greatest amount of rockfall for a 1×10^{-6} annual probability of exceedance ground motion. Two particular cases of the 50 analyzed show a larger amount of rockfall due to the fact that the two long, subvertical fracture sets strike at a low angle to the axis of the emplacement drift. This, coupled with the presence of closely spaced subhorizontal vapor phase partings or random sets, allows a number of roof and sidewall blocks to detach over a significant plan view area. The drift preferentially breaks out along the sidewalls since this is the location of highest induced stress along the tunnel periphery.

5.2. *Thermal-mechanical analysis*

Thermal-mechanical modeling was performed to define drift stability under combined in situ and thermally induced stresses. Temperatures within the rock mass are determined from thermal analysis conducted using the NUFT program, which accounts for the details of heat transfer mechanisms within the drift, including heat removal due to ventilation in the preclosure period. The NUFT thermal calculation considers a 1.45 kW/m initial linear heat load and 50-year preclosure ventilation with 90% of heat removed by ventilation. The NUFT approach is two-dimensional and, thus, assumes a cross section through a series of infinitely long emplacement drifts. Thus, this type of approach adequately represents the developing temperature

distribution around emplacement drifts located centrally within the repository. Fig. 13 presents the drift crown temperature history. The peak temperature was predicted to be 138°C at approximately 75 years, and reduced to below boiling after 1,000 years.

Rockfalls induced by thermal loading are found to be minor. Most of the damage, although little, occurs in the rock mass during the heating period. Less than 1 m^3 of rockfall is predicted within the 25-m tunnel simulated for all cases analyzed. There is little to no change on yielding and permanent deformation during the cool-down period. Sensitivity of rock thermal properties results shows an insignificant effect with varying rock thermal properties by one standard deviation.

For the combination of in situ, thermal and seismic loads, three example cases were chosen to cover the likely range of drift degradation. The thermal state with the highest level of rock temperature and thermally induced rock stress (i.e., 80 years after waste loading) was chosen. The initial state (before heating began) and the state after 80 years of heating coincide with extreme points on thermally induced stress paths at a number of locations around the emplacement drift. The state after 80 years was felt to be of greatest interest because already-completed analyses with no thermal loading provide the other extreme thermal condition. In summary, the impact of thermal loading in nonlithophysal rock is to stabilize the rock mass and reduce rockfall. The reason for this effect is that the rock mass expansion on heating induces tangential compression around the excavations. This compression tends to provide increased normal stresses to fractures, thus increasing their shearing resistance as well as minimizing joint opening during extensional loading during a seismic event. Thus, the most conservative thermal state, from a rockfall standpoint, is actually when the rock is at or near ambient temperature.

5.3. Sensitivity studies of the input parameters and model conditions

5.3.1. Fracture surface property variation and fracture strength degradation

The base-case joint properties, listed in Table 4, were based on the rotary shear tests of the cored rock specimens. Additional direct shear tests have been completed, and results from these tests are used to provide the range of shear strength variation tested in the sensitivity studies. With limited joint test results currently available and given the fact that the use of rotary shear devices in rock mechanics is not common, some of the

parameters in the base case, such as cohesion and dilation angle, were scaled down from the testing results for conservatism, to allow for an investigation of parameter sensitivity on rockfall development.

A range of joint properties, as shown in Table 6, was selected for the sensitivity study. The values for joint categories 1 to 3 were established based on the residual friction angle of 30° and three tiers of dilation angles. The dilation angles were selected within the range of reported test results. The results of these sensitivity studies show that the variation of joint mechanical properties is a secondary effect compared with the variation of fracture geometrical properties (i.e., fracture pattern). Results for the three categories are quite similar, irrespective of the variation of the mechanical properties used for each category. Joint category 4 is used to represent the degraded joint condition. The reduced joint strength parameters are estimated to be in the range of the residual, post-peak shear displacement state with joint cohesion reduced to zero and the joint friction angle reduced to 30°. Dilation angle is also conservatively presumed to be zero, considering that the asperities on fracture surfaces had been sheared off. The net result of these conservative assumptions is the potential for greater rockfall. The degraded joint strength and dilatational properties were applied in three 1×10^{-5} annual probability of exceedance seismic motion cases that represent the case with the greatest amount of rockfall, the median case, and the case producing no rockfall. The predicted number of detached rock blocks and the total rockfall volume show that only a slight increase in rockfall is predicted for the degraded state. Thus, potential time-related joint strength degradation has a minor impact on drift stability in nonlithophysal rock.

5.3.2. Rock bridge strength

Solid rock "bridges" between fractures were automatically generated as the extension of finite trace length fractures to form the distinct blocks in the 3DEC model. During a simulation, the stress conditions acting on these solid rock bridges are monitored, and failure in shear or tension can occur. Rock bridge damage either in shear slip or tensile separation appears to have a strong relationship with peak ground velocity. In general, less than 1% of the bridge area is damaged when subjected to 1×10^{-5} annual probability of exceedance ground motions, with about 5% bridge damage for 1×10^{-6} ground motions, reaching to 20% bridge damage for 1×10^{-7} ground motions. However, for certain large ground motions, much higher damage percentage is expected. Fig. 14 shows the correlation between the damage percentage and the peak ground velocity.

A range of bridge strength parameters, in terms of cohesion, friction angle, and tensile strength, was selected for the sensitivity study. This range of intact rock properties was derived from the results of triaxial testing of rock cores from the Tptpmn. A total of 3 categories were included to cover the possible range of variation for bridge strength parameters and was subject to 1×10^{-5} annual probability of exceedance motions. The joint strength parameters are used for category 1 to represent the extreme case where all the bridges are sheared-off to become fractures. The mean values of the intact Tptpmn strength parameters are used for category 2. The mean-plus-one standard deviation values determined from triaxial testing are assigned as the strength parameters for category 3. This category represents the upper bound for the rock bridge strength. The results show that within the range of variation for the intact strength parameters (categories 2 and 3), rock bridge strength parameters have an insignificant impact on rockfall prediction. However, if all rock bridges are sheared-off, as represented by category 1, a significant increase of rockfall volume occurs with smaller rock block size.

5.3.3. Intact block failure response under low-probability ground motions

At the lower seismic hazard levels, the ground motions show extreme PGV levels, ranging from 2.44 m/s at the 1×10^{-6} to 5.35 m/s at the 1×10^{-7} annual exceedance probabilities. The calculations and estimates of dislodged block masses and volumes assumed that the rock blocks were, in general, elastic. The only block failure that was allowed was breakage of solid rock "bridges" that occur along the extension of fracture planes, between the end of the fracture and its possible termination against adjacent fractures. Thus, in the current model, it is possible for a block to split into several smaller blocks if the seismic stresses are sufficient to fail the rock bridge in shear or in tension.

A sensitivity study of rock bridge strength provides a conservative assessment of the case in which the tensile strength of the rock bridges is assumed to be zero. This case effectively represents the condition in which the tensile strength of the rock mass is conservatively assumed to be zero as no rock bridges exist. These analyses indicate that the rockfall volume increases between 3 to 5 times for the 1×10^{-6} and the 1×10^{-7} cases. The drift degradation profile for the base case rock bridge strength and the case in which the rock bridge tensile strength is set to zero are shown in Fig. 15 for the 1×10^{-6} ground motions. As seen in this

figure, the rockfall increases significantly with the assumption of zero rock bridge tensile strength, but total collapse is not evident.

5.4. Validation of the drift-scale modeling method for nonlithophysal rock using the 3DEC program

The modeling of the nonlithophysal rock requires use of a three-dimensional, discontinuum modeling approach. A validation strategy was adopted based on demonstrating that the mechanical response of the fractures, which control the stability of the tunnel under shaking, function properly by corroboration with laboratory data. The rockfall component results from 3DEC are compared to an explosively loaded, scaled tunnel stability experiment in jointed rock. Additionally, results from the nonlithophysal rockfall model are compared to an alternative numerical model. Finally, an external expert technical review is used as a method for validation of the overall modeling approach for representation of nonlithophysal rock.

The details of the validation comparisons are given in *Drift Degradation Analysis* [6]. The validation tests demonstrate the following:

- Analyses indicate that the 3DEC program is able to represent dynamic boundary conditions and wave transmission through the material in an accurate fashion.
- The comparison of the 3DEC program to the results of direct shear testing on fractures from the Tptpmn shows that 3DEC is able to adequately reproduce the shear constitutive response of the cooling and vapor-phase altered fractures. Use of sensitivity analyses to bound fracture shear stiffnesses in the vapor-phase altered fractures is warranted, although analysis indicates that the use of tangent stiffnesses and a softening joint mechanical model (the default used in the 3DEC model) appears to be conservative in nature, resulting in more rockfall.
- The ability of 3DEC to represent the complex problem of an explosively loaded tunnel in jointed rock was tested via comparison to a scaled field experiment in limestone. The field experiment tested several capabilities of the program, including:
  - The predictive capability of the nonlithophysal rockfall model as implemented in 3DEC for structures in jointed rock was demonstrated by comparing predictions with the results of a large jointed-rock test specimen that involved dynamic loading and large strain of a lined cylindrical opening. Based on this

validation case, 3DEC can reasonably simulate the wave transmission through the jointed rock, the stress change in the rock mass resulting from the dynamic excitation, and the large strain and permanent deformation of a tunnel in jointed rock and its internal support.

- 3DEC demonstrated the ability to represent complex dynamic boundary conditions.
- 3DEC accurately predicted the final shape of the deformed liner.
- 3DEC accurately predicted the arrival time of the stress waves, thus validating the wave transmission simulation through the jointed rock.
- 3DEC accurately predicted the stress magnitudes and wave shape at several of the monitoring points. Wave reflections disturbed this prediction in some locations. Note that the inclusion of random gaps in the model adds difficulty in matching the stresses at specific locations.
- The 3DEC model as shown compared very favorably with the physical experiment and demonstrated the ability to represent reasonably the dynamic response of a fractured media.

• The overall adequacy of the modeling approach and the specification of property ranges have been validated by corroboration with the results of an alternative numerical model and by external technical review.

6. Conclusions

This paper summarizes the geologic, laboratory, field, and numerical analysis work related to the mechanical degradation of the nonlithophysal rock mass surrounding the emplacement drifts of a proposed geologic repository at Yucca Mountain. A drift degradation model for nonlithophysal rock was developed using the three-dimensional discontinuum code 3DEC for the planned repository emplacement drift at Yucca Mountain. This model includes the development of fracture patterns generated from multiple sampling from a synthetic rock mass volume that contains a realistic fracture population based on field mapping data. Site-specific ground motion time histories, with annual probabilities of exceedance ranging from 1×10^{-4} to 1×10^{-7}, are included in the model.

Degradation in the nonlithophysal units is primarily controlled by geologic structure. Ground motion with an annual probability of exceedance of 1×10^{-4} results in minor drift damage due to rockfall even with the

assumption of unsupported drift openings. Ground motions with annual probabilities of exceedance from 1×10^{-5} to 1×10^{-7} result in varying extent of drift damage due to rockfall, with localized areas of rock failure sufficient to cover the drip shield.

Thermal-mechanical analyses were conducted using both a base case set of thermal properties and a sensitivity case considering the values for thermal conductivity and specific heat one standard deviation smaller than the mean. The transient temperature field around the repository was calculated using 90% and 70% ventilation heat removal efficiencies. There was minimal rockfall predicted at any time for the thermal only scenario (i.e., no seismic loading) for the cases analyzed. When thermal stresses were considered in combination with the stresses resulting from postclosure seismic ground motion, it is clearly shown that thermal loading reduces the amount of rockfall.

Drift stability due to the effect of time-dependent rock joint degradation is assessed based on a reduction of joint cohesion and friction angle. The reduced joint strength parameters are estimated to be in the range of the residual state with joint cohesion reduced to zero and the joint friction angle reduced to 30°. Dilation angle is also reduced to zero considering that the asperities on fracture surfaces had been sheared off. The degraded joint strength and dilational properties were applied, while a slight increase in rockfall is predicted for the degradated state. Overall, joint strength degradation has a minor impact on drift stability.

A validation strategy was adopted based on demonstrating that the mechanical response of the fractures, which control the stability of the tunnel under shaking, function properly by corroboration with laboratory data. The rockfall component results from 3DEC are compared to an explosively loaded, scaled tunnel stability experiment in jointed rock. Additionally, results from the nonlithophysal rockfall model are compared to an alternative numerical model. Finally, an external expert technical review is used as a method for validation of the overall modeling approach for representation of nonlithophysal rock. The model development activities and post-development validation activities described establish the scientific bases for the drift-scale modeling of nonlithophysal rock. Based on this, the drift degradation model is considered to be sufficiently accurate and adequate for the intended purpose and to the level of confidence required by the models' relative importance to the potential performance of the repository system.

Acknowledgements

This work was performed and funded under Department of Energy contract DE-AC28-01RW12101 for the Civilian Radioactive Waste Management System (CRWMS). Bechtel SAIC Company, LLC is the prime contractor for CRWMS.

References

[1] Damjanac B, Board M, Lin M, Kicker D, Leem J. Mechanical degradation of emplacement drifts at Yucca Mountain—A modeling case study. Part II: Lithophysal rock. Int J Rock Mech Min Sci 2006;43:#–#. (in progress)

[2] Bechtel SAIC Company. Yucca Mountain site description. Las Vegas, Nevada: Bechtel SAIC Company Report TDR-CRW-GS-000001 REV 02 ICN 01, 2 volumes; 2004.

[3] Bechtel SAIC Company. Subsurface geotechnical parameters report. Las Vegas, Nevada: Bechtel SAIC Company Report 800-K0C-WIS0-00400-000-00A; 2003.

[4] Civilian Radioactive Waste Management System Management & Operating Contractor. Geology of the Exploratory Studies Facility Topopah Spring loop. Las Vegas, Nevada: CRWMS M&O Report BAB000000-01717-0200-00002 REV 01; 1998.

[5] Mongano GS, Singleton WL, Moyer TC, Beason SC, Eatman GLW, Albin AL, Lung RC. Geology of the ECRB Cross Drift — Exploratory Studies Facility, Yucca Mountain Project, Yucca Mountain, Nevada. Denver, Colorado: US Geological Survey Deliverable SPG42GM3; 1999.

[6] Bechtel SAIC Company. Drift degradation analysis. Las Vegas, Nevada: Bechtel SAIC Company Report ANL-EBS-MD-000027 REV 03; 2004.

[7] Dershowitz, WS. Rock joint systems. PhD thesis, Massachusetts Institute of Technology; 1984.

[8] Itasca Consulting Group. Itasca software–cutting edge tools for computational mechanics. Minneapolis, Minnesota: Itasca Consulting Group; 2002.

[9] Bechtel SAIC Company. Peak ground velocities for seismic events at Yucca Mountain, Nevada. Las Vegas, Nevada: Bechtel SAIC Company Report ANL-MGR-GS-000004 REV 00; 2005.

[10] Bechtel SAIC Company. Sampling of stochastic input parameters for rockfall calculations and for structural response calculations under vibratory ground motion. Las Vegas, Nevada: Bechtel SAIC Company Report ANL-EBS-PA-000009 REV 01; 2004.

Table 1
General characteristics of fracture sets in the nonlithophysal unit

Set	Observed orientation, azimuth/dip (°)	Median spacing (m)	Median trace length (m)	Comment
1	120/84	0.48	3.3	Rough to smooth, planar
2	215/88	1.08	2.9	Smooth but curved
3	302/38	3.40	3.7	Random fractures with generally flat to moderate dip
4	329/14	2.46	3.5	Vapor-phase partings, rough, cohesive with coating minerals, planar

Table 2
Comparison of data from field mapping and FracMan output for the Tptpmn

Set	Observed orientation (strike/dip)	FracMan orientation (strike/dip)	Median inter-fracture distance (m)		Median trace length from full periphery geologic maps (m)	Trace length median from FracMan (m)
			Observed	FracMan		
1	120/84	125/84	0.48	0.79	3.3	2.8
2	215/88	214/86	1.08	1.29	3.1	2.9
3	302/38	299/43	3.40	3.16	3.6	3.7
4	329/14	327/08	2.46	1.48	3.4	3.5

Table 3
Base-case material properties for 3DEC analysis

Material property		Value
Joint strength properties	Joint cohesion (MPa)	0.1
	Joint friction (°)	41.0
	Joint dilation (°)	0
	Joint normal stiffness, K_n (MPa/m)	5×10^4
	Joint shear stiffness, K_s (MPa/m)	5×10^4
Intact rock deformation properties	Young's modulus (GPa)	33.0
	Poisson's ratio	0.21
	Bulk modulus (GPa)	19.2
	Shear modulus (GPa)	13.6
Intact bridge strength properties	Cohesion (MPa)	47.2
	Friction angle (°)	42.0
	Tensile strength (MPa)	11.6

Joint dilation is set to zero for the base-case analysis. With no dilation, joints are modeled as perfectly planar and smooth, resulting in a conservative (i.e., higher) estimation of rockfall.

Table 4
Peak ground motion parameters

Annual hazard level	Ground motion component	Peak acceleration (g)	Peak velocity (cm/s)	Peak displacement (cm)	Seismic induced stress corresponding to peak velocity (MPa)
1×10^{-4}	H1	0.39	38.38	44.44	2.20
	H2	0.37	43.78	45.3	2.51
	V	0.47	47.51	31.73	4.50
1×10^{-5} (Set 1)	H1	2.77	104.58	20.06	6.00
	H2	2.50	83.31	14.37	4.78
	V	2.63	70.88	13.00	6.71
1×10^{-6} (Set 1)	H1	7.42	244.14	26.76	14.00
	H2	6.74	195.41	26.78	11.21
	V	4.90	111.29	13.75	10.54
1×10^{-7} (Set 1)	H1	16.28	535.26	58.68	30.00
	H2	14.79	428.42	58.72	24.57
	V	13.15	298.44	36.86	28.25

Table 5
Comparison of rockfall statistics

Statistic	Ground motion annual probability of exceedance			
	1×10^{-4}	1×10^{-5}	1×10^{-6}	1×10^{-7}
Runs completed	32	50	50	44
Total number of rockfall	428	1,764	2,797	3,387
Total volume of rockfall (m^3)	39.4	255.4	497.7	705.2
Total length of drift simulated (m)	800	1,250	1,250	1,100
Number of blocks per km	535	1,414	2,238	3,079
Volume of rockfall per km (m^3/km)	49.3	204.3	398.2	641.1

Table 6
Four categories of joint properties used in the sensitivity study

Joint category	Joint cohesion (Pa)	Joint dilation angle (°)	Peak friction angle (°)	Joint shear stiffness (Pa/m)	Joint normal stiffness (Pa/m)
1	1.0×10^5	1.4	31.4	5.3×10^9	7.2×10^{10}
2	1.0×10^5	4.4	34.4	1.1×10^{10}	9.4×10^{10}
3	1.0×10^5	11	41	1.7×10^{10}	1.2×10^{11}
4	0	0	30	5.3×10^9	7.2×10^{10}

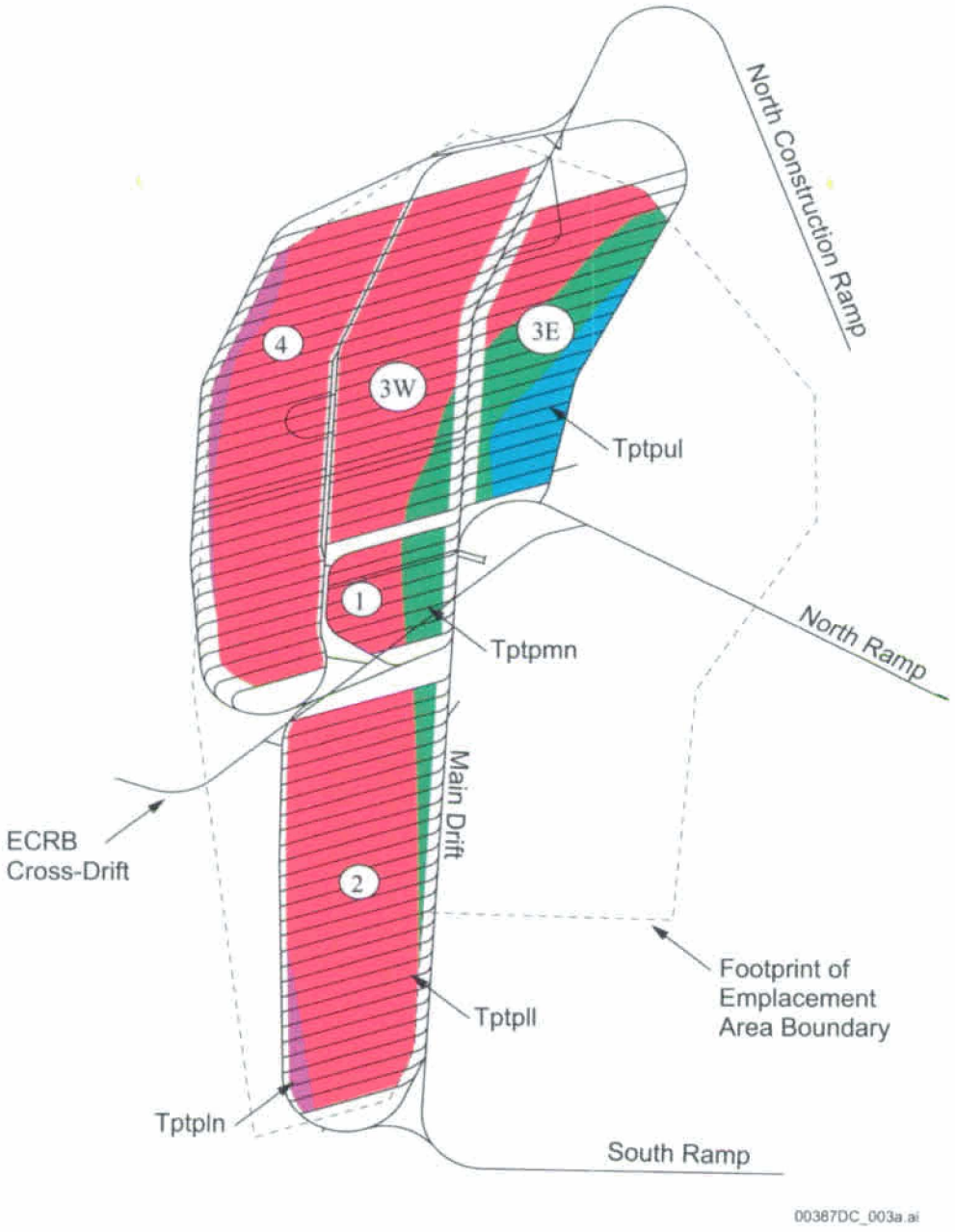

Fig. 1. Proposed repository layout in plan view showing intersections of geologic subunits with emplacement drifts. The repository includes 5 panels: Panels 1, 2, 3E, 3W, 4, and 5.

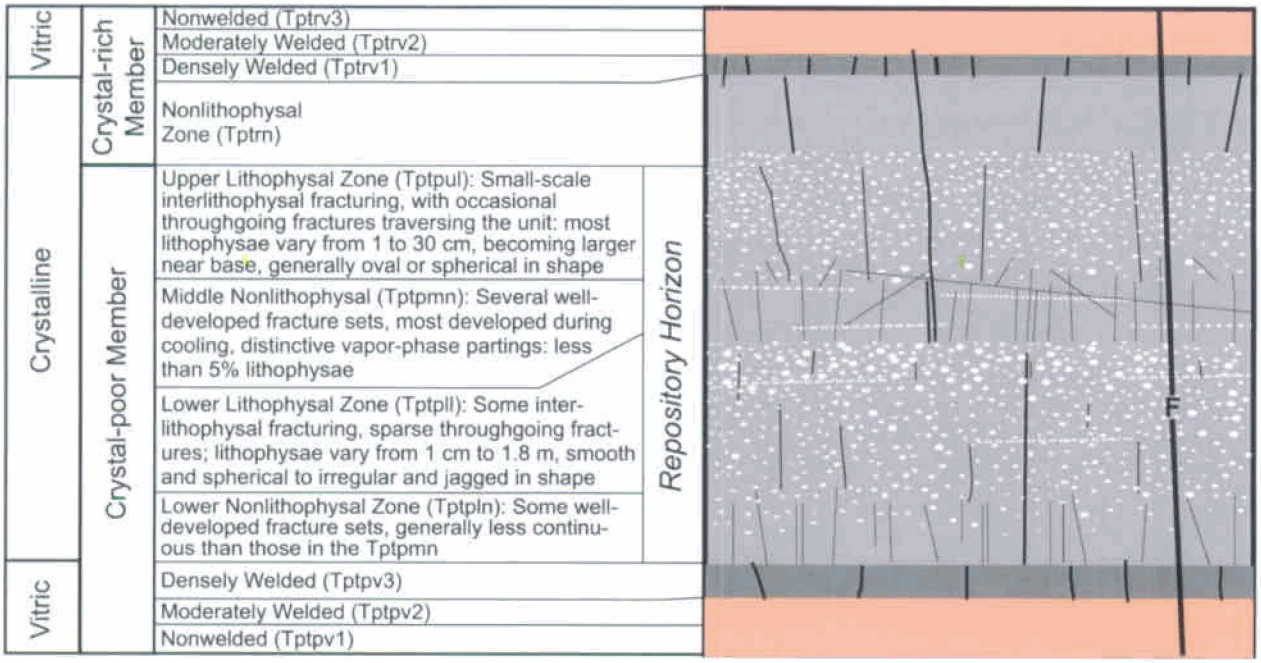

Diagrammatic Cross Section of the Topopah Spring Tuff Illustrating Relative Discontinuity Densities and Orientations: This figure indicates how fractures, faults, and lithophysae are typically distributed through the ignimbrite.

Fig. 2. Structure of the Topopah Spring Tuff showing relative relationship between fracturing and lithophysae in major flow subunits.

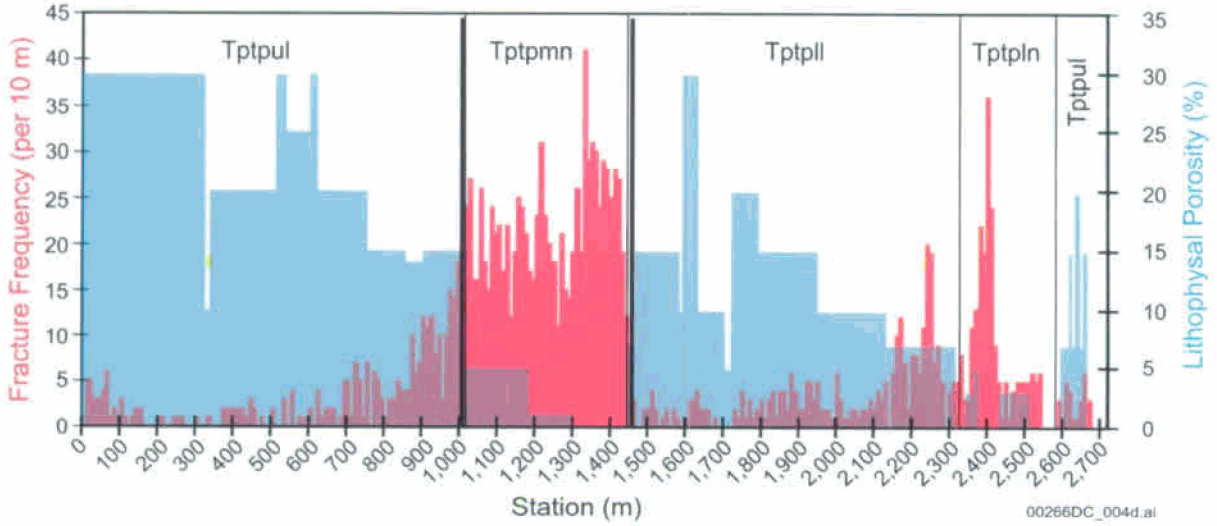

Fig. 3. Composite plot of fracture frequency and lithophysal porosity as a function of distance along the ECRB Cross-Drift.

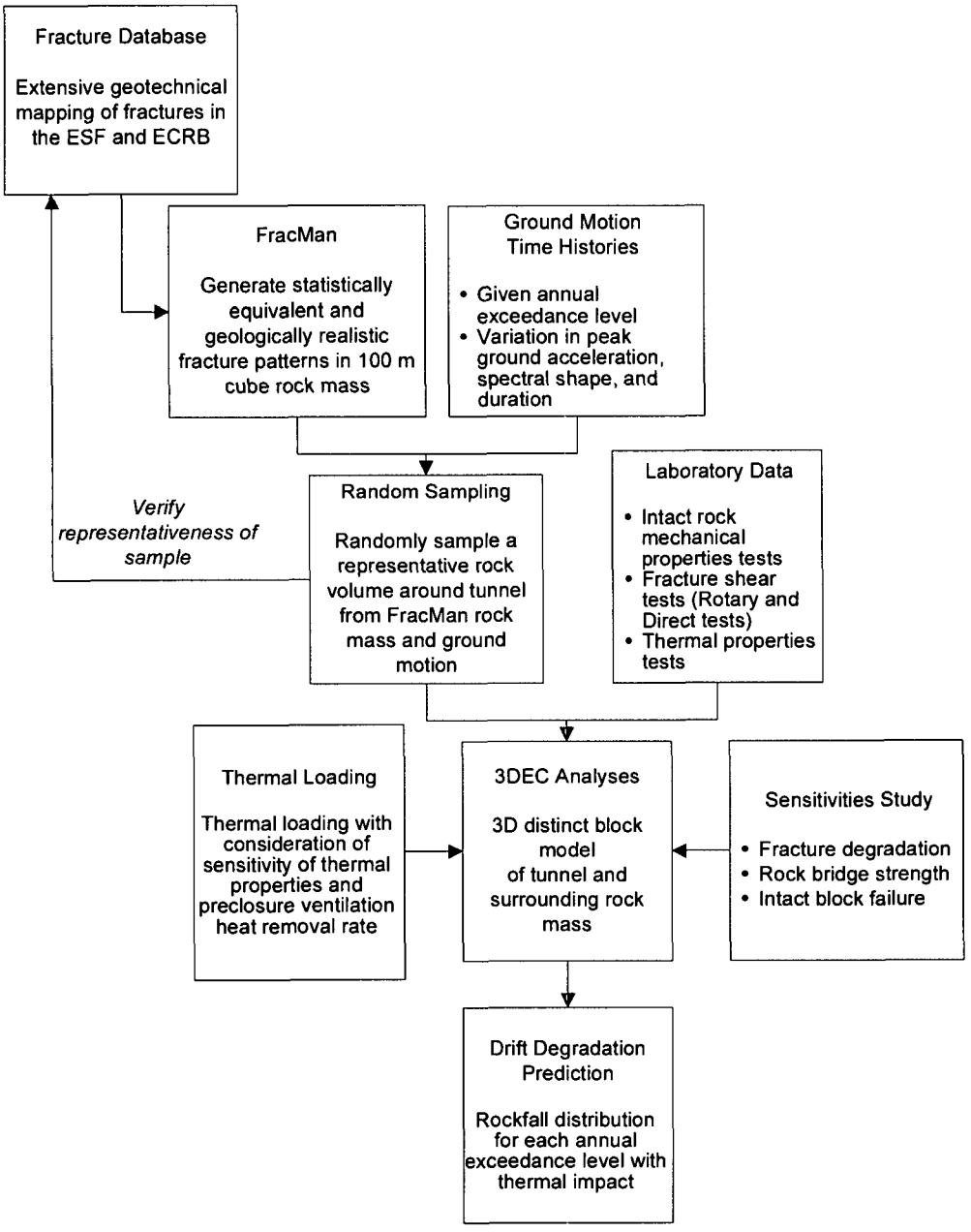

Fig. 4. Approach of drift degradation and rockfall analyses for nonlithophysal rock.

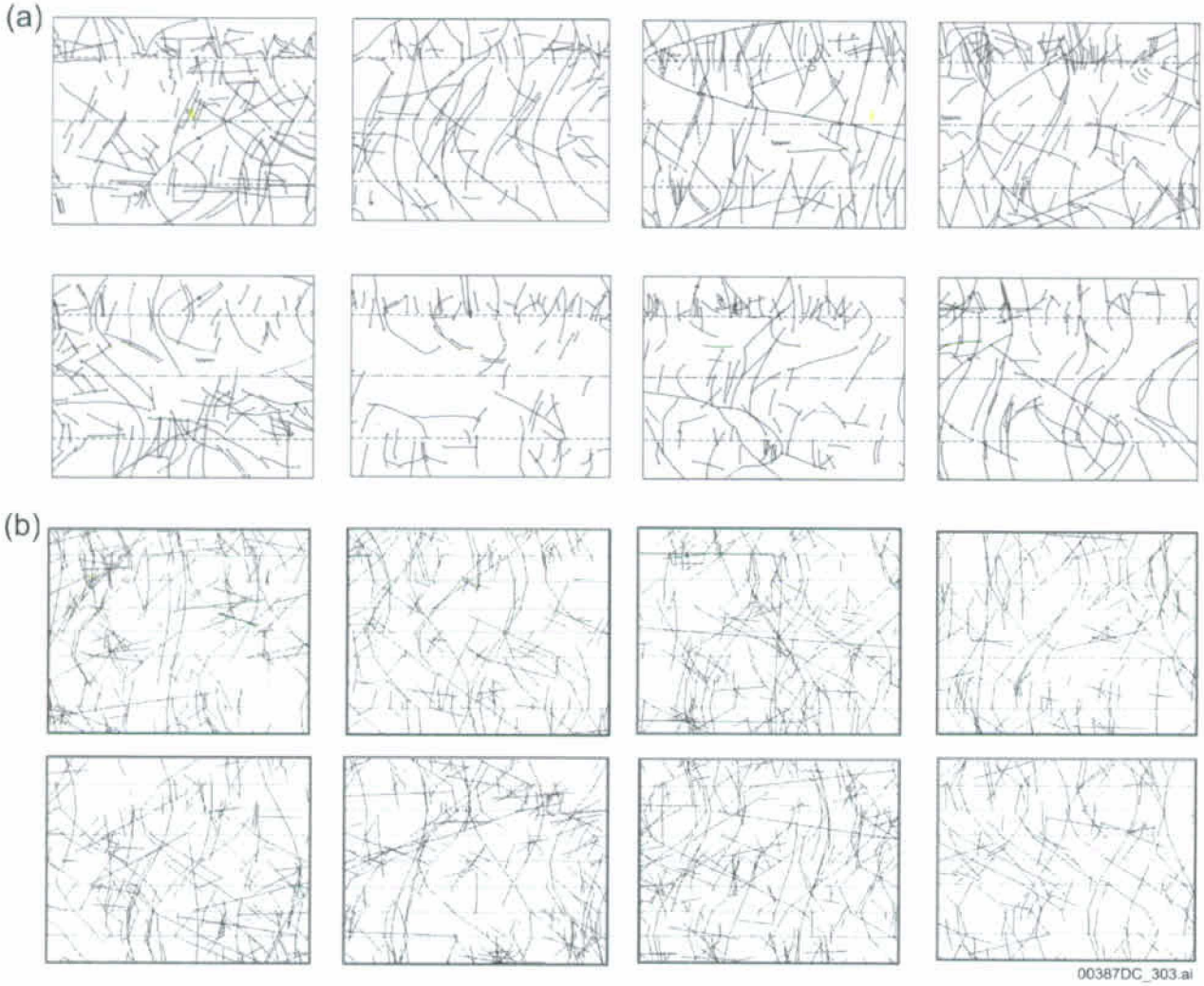

Fig. 5. Comparison of (a) full periphery geologic maps from the Tptpmn in the Exploratory Studies Facility with (b) simulated full periphery geologic maps from the FracMan cube.

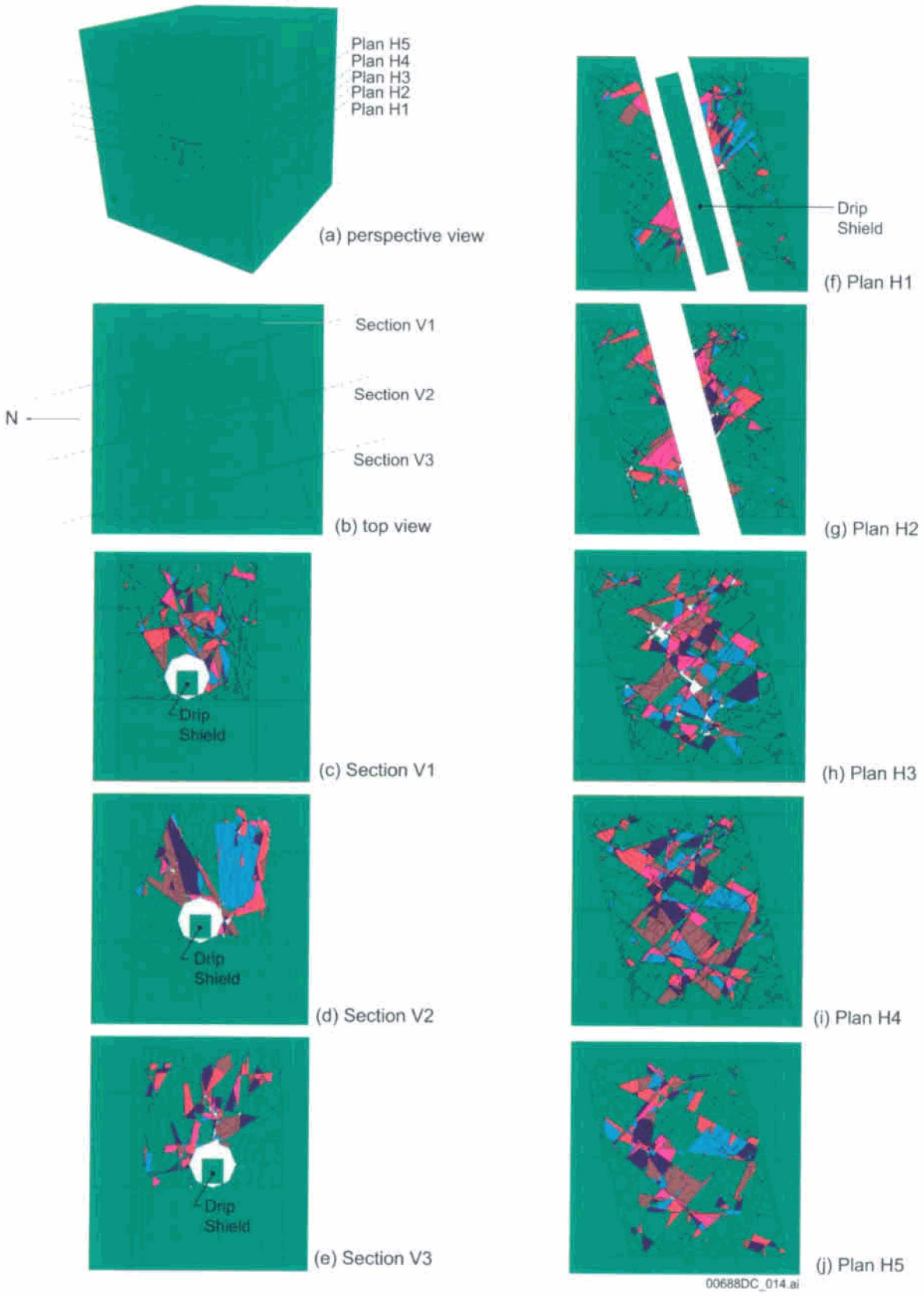

Fig. 6. 3DEC model geometry and cross sections.

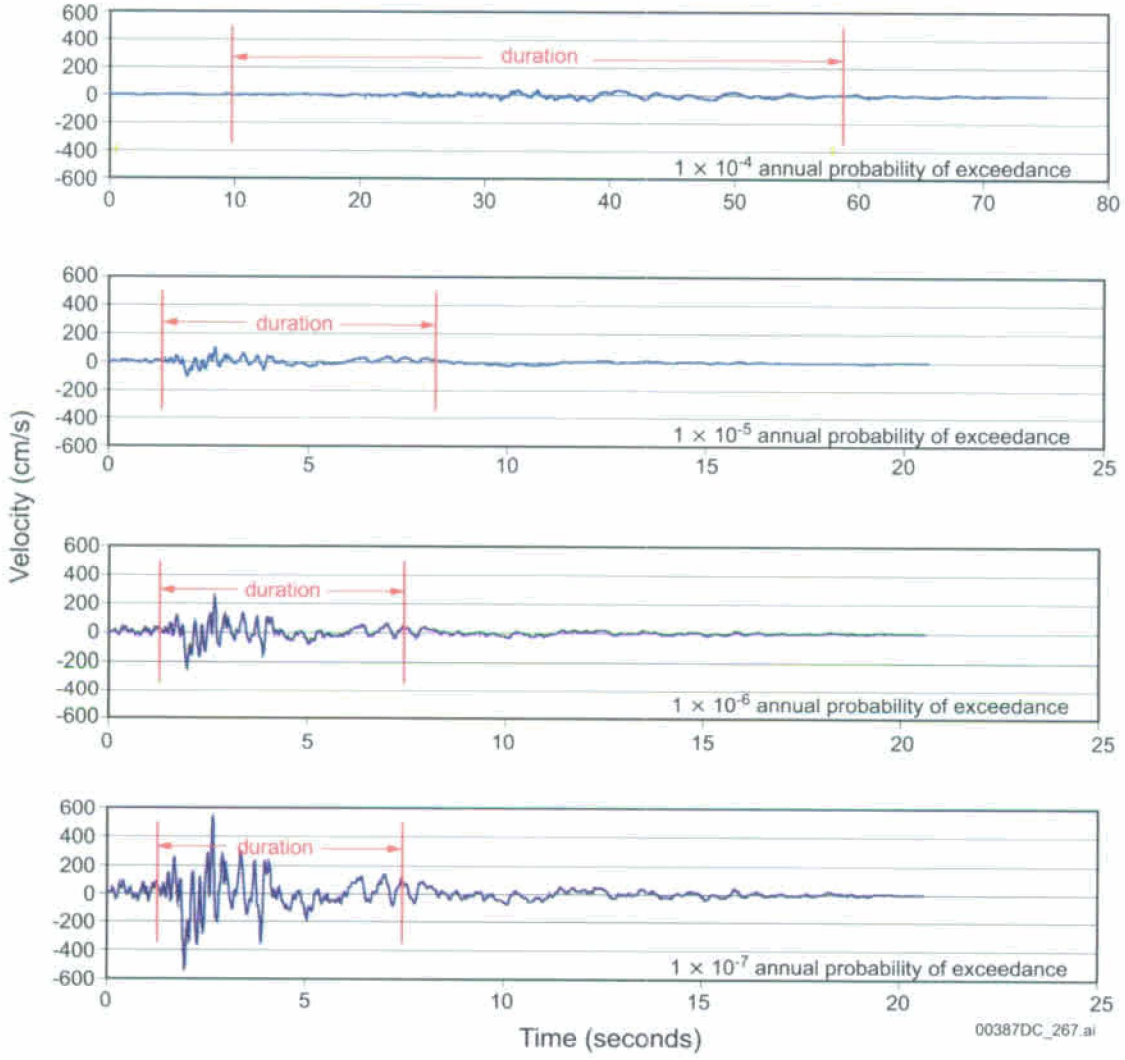

Fig. 7. Examples of ground velocity time histories (H1) with truncated duration for analysis.

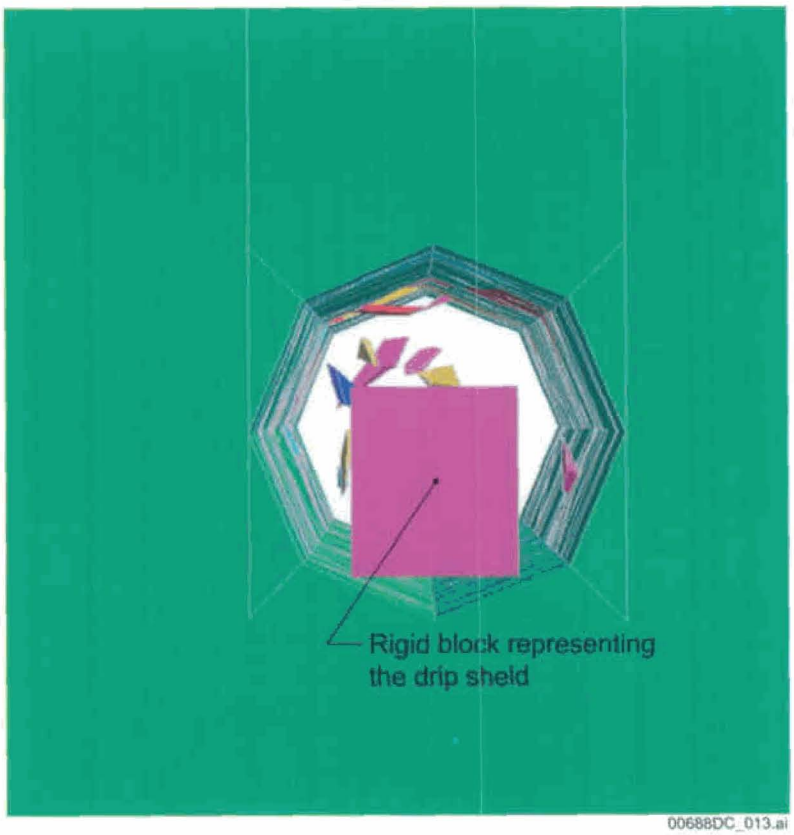

Fig. 8. 3DEC simulation of rockfall impact to the drip shield. The 5.5-m diameter drift is represented with a three-dimensional octagonal shape shown projected into the 25-m × 25-m × 25-m model volume. The rigid drip shield block is affixed to the tunnel invert.

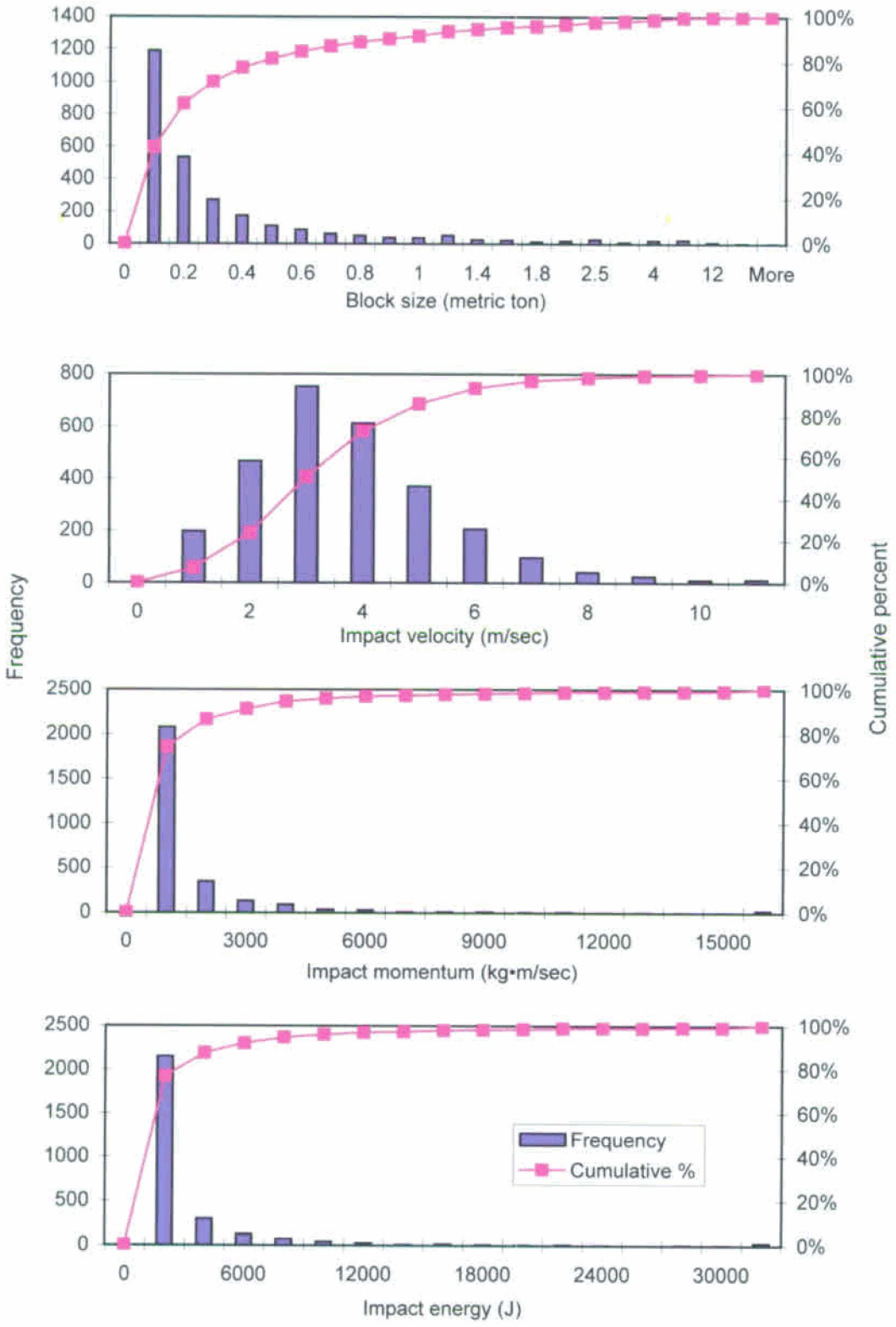

Fig. 9. Summary histograms for seismic analyses with 1×10^{-6} annual probability of exceedance hazard: (a) block size (b) relative impact velocity (c) impact momentum, and (d) impact energy.

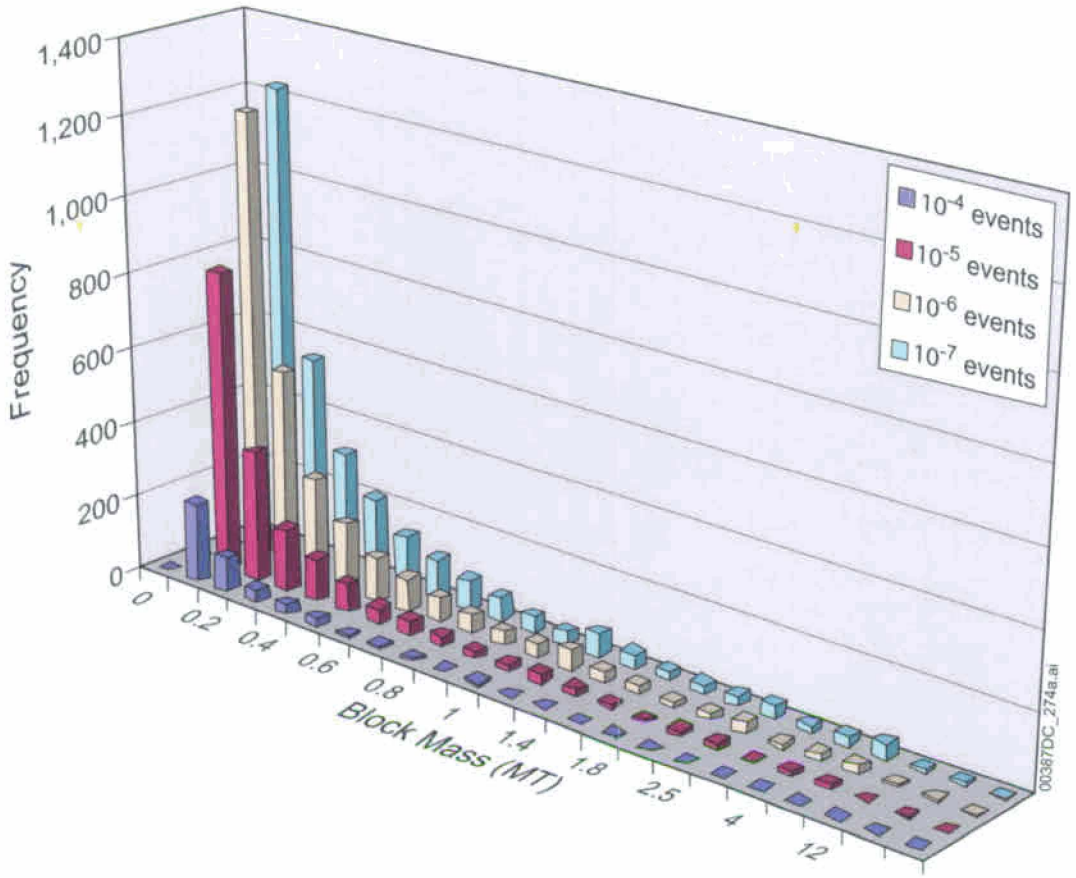

Fig. 10. Comparison of histograms of block mass from preclosure and postclosure ground motions.

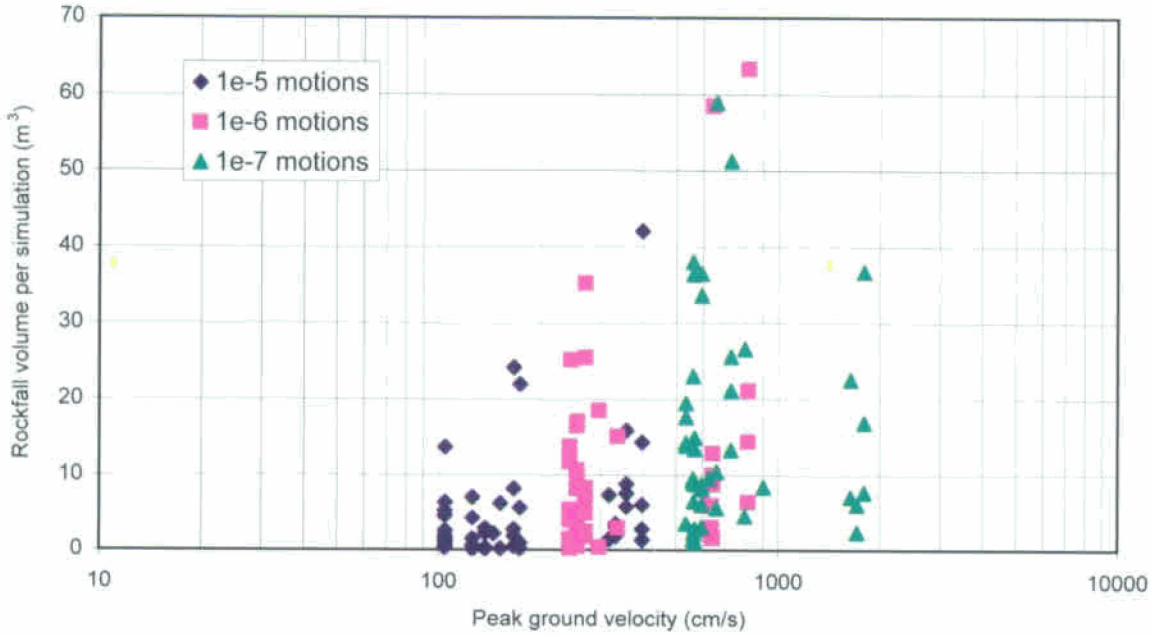

Fig. 11. Rockfall volume versus peak ground velocity

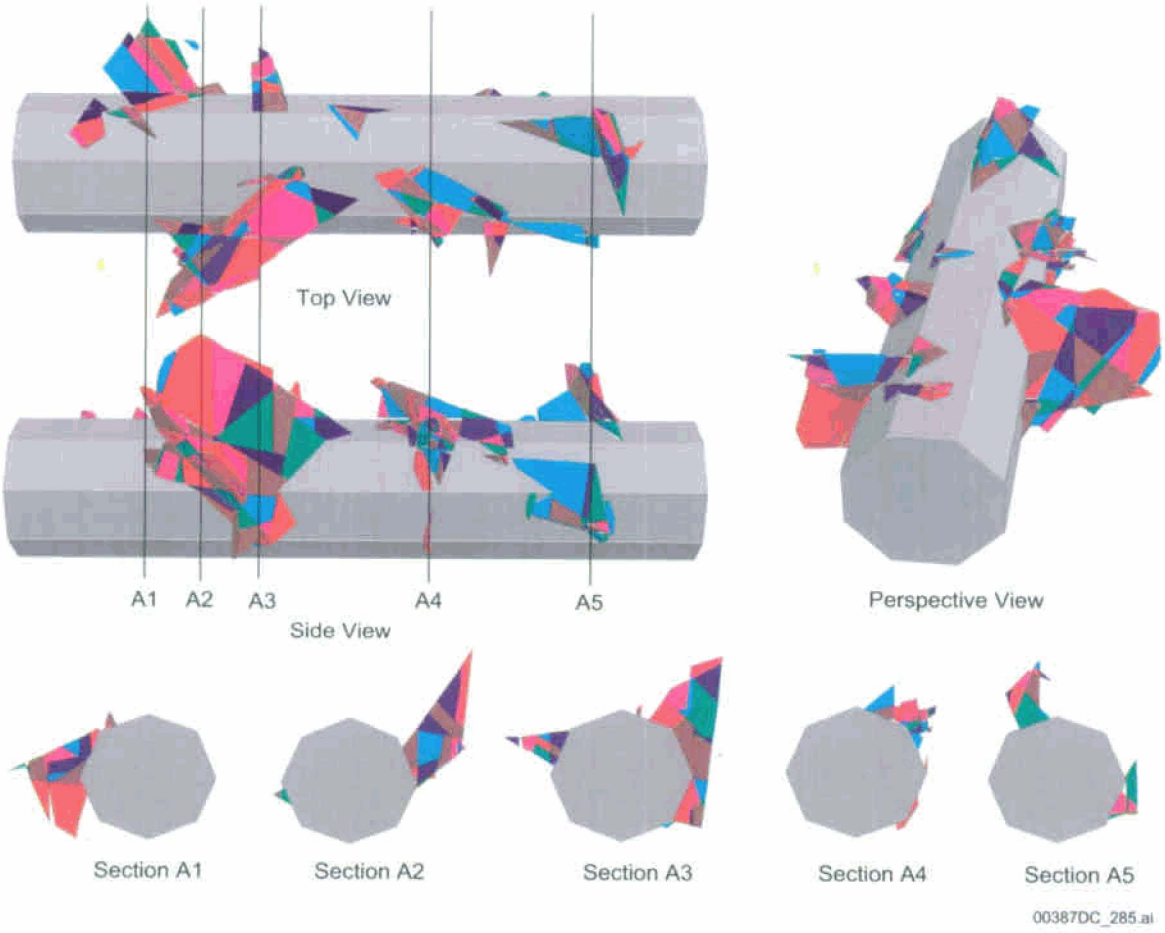

Fig. 12. Drift profile for 1×10^{-6} hazard level, case with greatest amount of rockfall.

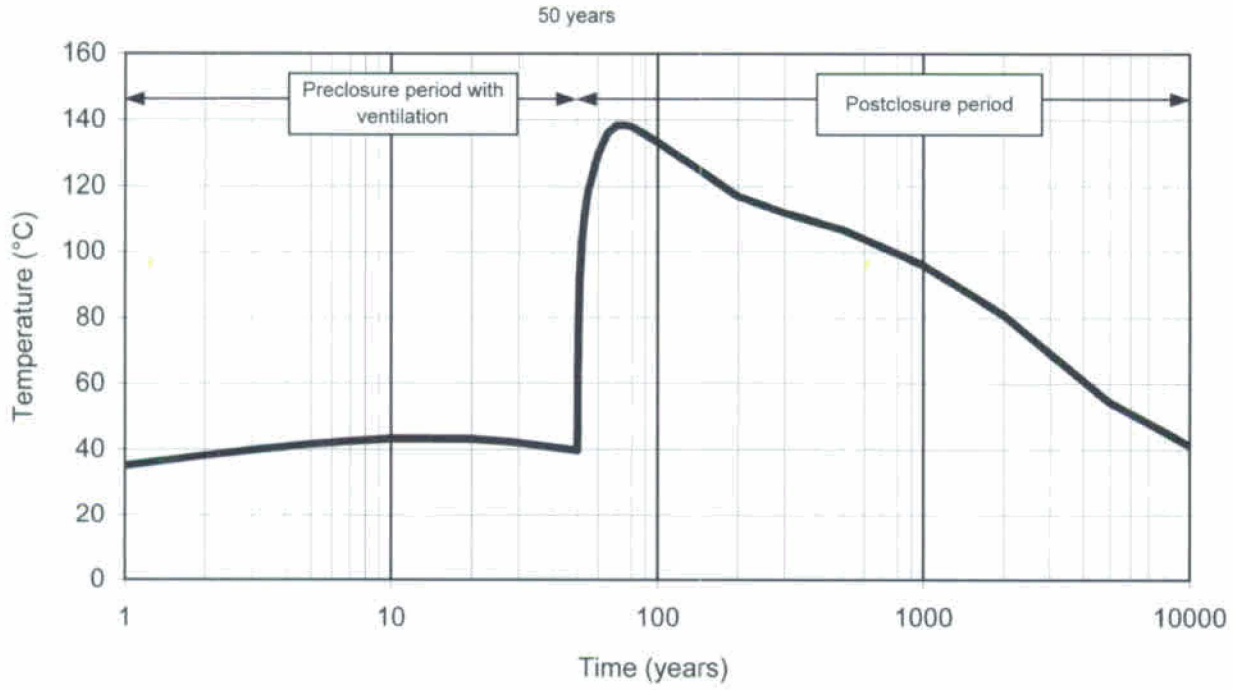

Fig. 13. Predicted drift crown temperature history.

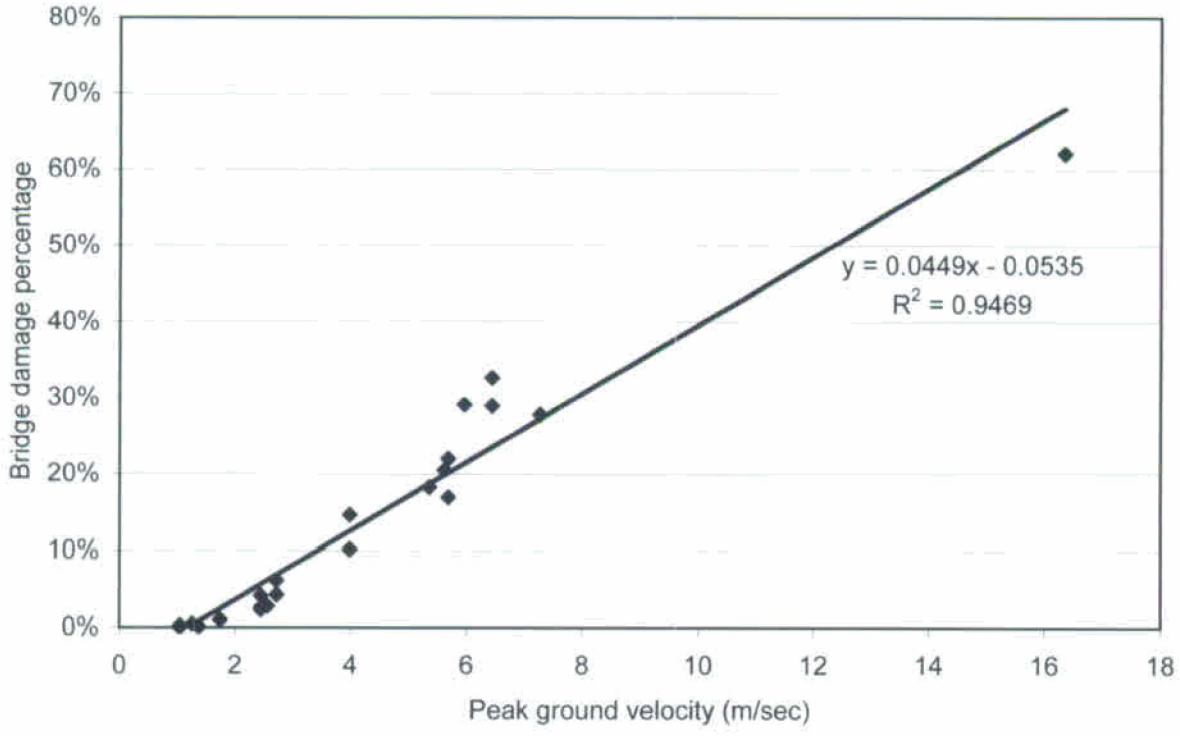

Fig. 14. Correlation of rock bridge damage percentage and peak ground velocity.

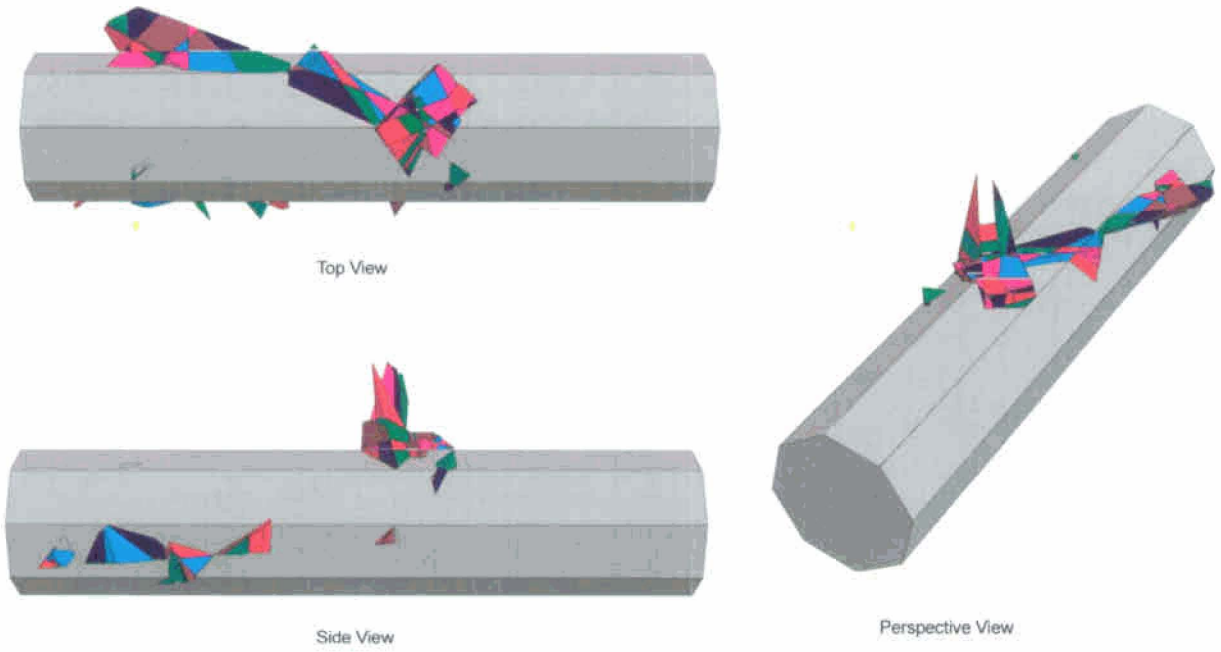

(a)

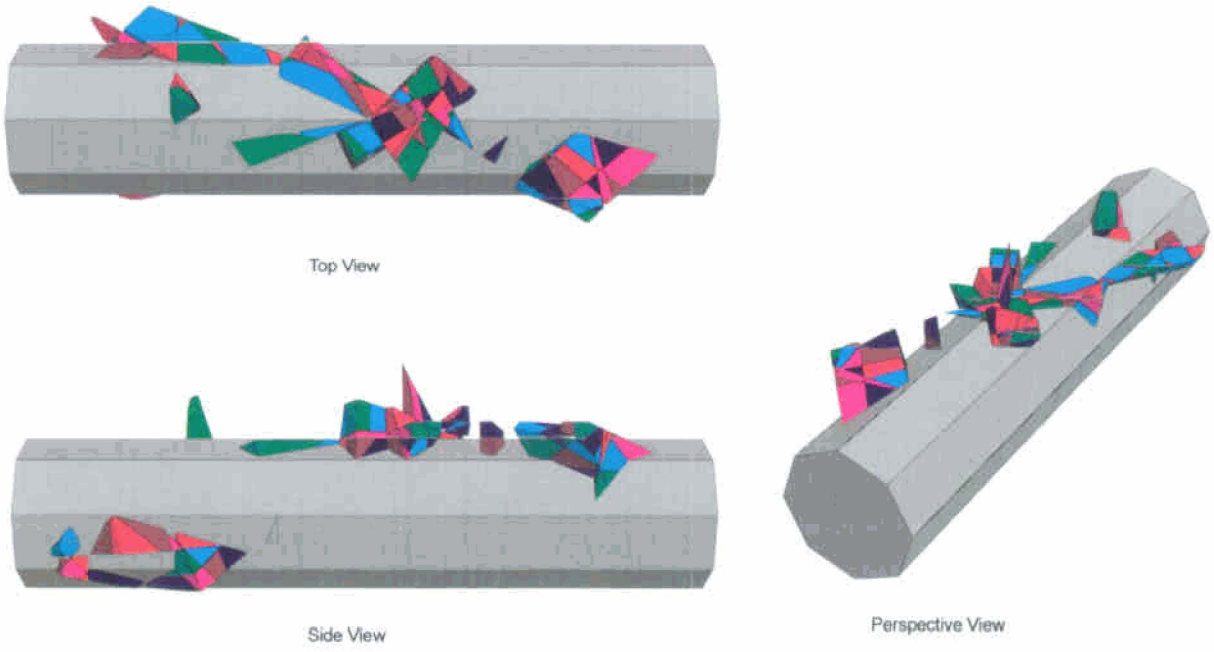

(b)

Fig. 15. Three-dimensional visualization of rockfall for the median rockfall condition: (a) base case and (b) low rock bridge strength properties, 1 × 10–6 ground motion.